BIOPHYSICS

The mechanical response of vinculin

Xuyao Liu[1,2]†, Jingzhun Liu[1,2]†, Yinan Wang[1,2]†, Mingxi Yao[3], Karen B. Baker[4], Benjamin Klapholz[5], Nicholas H. Brown[5], Benjamin T. Goult[4,6]*, Jie Yan[1,2,7]*

Vinculin is a mechanosensitive adaptor that links actin to cell-matrix and cell-cell adhesions. Known as a mechanoeffector, it is recruited to adhesion sites under force via mechanotransducers talin and α-catenin. Here, we examine vinculin's mechanical properties to assess its role as a mechanotransducer. We find that at physiological loading rates, vinculin domains unfold at forces of 5 to 15 pN and refold rapidly when forces drop to 1 pN. This behavior is reminiscent of force-dependent switches in talin and α-catenin, suggesting vinculin domains also function as molecular switches. Unfolding induces large extension changes up to 150 nm in steps of 20 to 30 nm. These findings reveal that vinculin exhibits a previously unrecognized mechanical response, with dynamic folding/unfolding under force acting as a buffering mechanism. Given its role as a scaffold for many proteins, this mechanosensitive behavior supports a model where vinculin functions directly as a mechanotransducer, recruiting binding partners in a force-dependent manner.

INTRODUCTION

In recent years, there has been growing appreciation that cells not only respond to the chemical signals in their environment, but also to mechanical signals, such as the stiffness of the tissue and surrounding extracellular matrix (ECM) (*1*, *2*). Sensing the mechanical environment requires mechanotransducers: molecules that can convert mechanical forces into chemical changes within the cell. A current paradigm for mechanotransduction is provided by the mechanotransducers talin and α-catenin, which recruit the mechanoeffector vinculin in a force-dependent manner (*3*–*5*).

The force-dependent recruitment of vinculin requires the mechanical unfolding of domains within talin and α-catenin, key cytoskeletal linkers at the adhesive junctions mediating cell-ECM and cell-cell adhesion, respectively (*6*, *7*). This occurs because the vinculin binding sites (VBSs) are buried within the folded α-helical bundles and are exposed by force unfolding these domains. Thus, these domains function as mechanical switches, as they bind some proteins in their folded state and others in their unfolded state (*8*). Vinculin is one of the best characterized mechanoeffectors, as its recruitment to sites of cell adhesion is force dependent.

The interaction of vinculin with talin and α-catenin is not simply regulated by the exposure of VBSs as vinculin itself can also adopt closed and open conformations, altering its interactions with its binding partners. Vinculin consists of a number of domains comprised of bundles of α helices. The number of these bundles varies from six to eight, depending on the species, and, in some cases, pairs of bundles share an extended α helix, thereby forming a domain. Thus, vertebrate vinculin consists of domains D1 (bundles 1 and 2, D1A and D1B), D2 (bundles 3 and 4, D2A and D2B), D3 (bundles 5 and 6, D3A and D3B), D4 (bundle 7), an unstructured proline-rich linker, and a conserved five-helix bundle, vinculin tail, Vt (bundle 8) at the C terminus. The major interactions with vinculin reported to date involve D1, which binds VBS, the linker, which binds SH3 domain–containing partners such as CAP and p130Cas (*9*), and Vt, which binds actin. α-Catenin is a paralog of vinculin, with a similar structure, and the bulk of talin is also formed of helical bundles, some four-helix bundles and the majority with the addition of a fifth helix (*10*). Interdomain interactions within the vinculin head organize it into a pincer-like structure (Fig. 1B) (*11*, *12*).

Vinculin exists in equilibrium between closed and open conformations. In the closed conformation, it does not bind VBSs or actin (*13*) due to an autoinhibitory interaction between the head and tail domains (*14*, *15*). The open conformation is able to engage with talin/α-catenin and actin and is stabilized by these interactions (*16*, *17*). Force strengthens these interactions, as observed in cells (*18*). When force is reduced, the mechanosensitive interactions weaken and vinculin disengages and returns to its closed conformation. The importance of this regulatory mechanism was highlighted by the observation that, in *Drosophila*, expression of constitutively open vinculin is more detrimental than removing vinculin (*19*).

Vinculin binding to actin enables its role in focal adhesion (FA)–mediated mechanotransduction (*13*, *20*–*25*), and down-regulation of vinculin leads to disruptions in cell rigidity sensing, cell adhesion, cell growth, and migration, which in turn contribute to cancer metastasis (*26*–*28*). Loss of vinculin has also been found to break the balance in skin stem cell differentiation (*29*) and has been linked to both dilated and hypertrophic cardiomyopathies in patients (*30*–*32*).

Active vinculin thus forms a mechanical linkage between the VBS-binding D1 domain at one end and the actin-binding Vt domain at the other end (Fig. 1C). As a result, actomyosin contraction will exert force on the other domains of vinculin. The key question we wished to address here is, in addition to being a key mechanoeffector of the mechanotransducing proteins talin and α-catenin, could vinculin also be a mechanotransducer, regulating the binding to its partners in a force dependent manner? To gain insights into this question, it is essential to quantify the mechanical responses of the tension-bearing domains and linker regions of vinculin during physiologically relevant stretching processes. Based on these responses,

[1]Department of Physics, National University of Singapore, Singapore 117542, Singapore. [2]Mechanobiology Institute, National University of Singapore, Singapore 117411, Singapore. [3]Department of Biomedical Engineering, Southern University of Science and Technology, Shenzhen 518055, P. R. China. [4]School of Biosciences, University of Kent, Canterbury CT2 7NJ, UK. [5]Department of Physiology, Development, and Neuroscience, University of Cambridge, Downing Street, Cambridge CB2 1DY, UK. [6]Department of Biochemistry, Cell and Systems Biology, Institute of Systems, Molecular and Integrative Biology, University of Liverpool, Crown Street, Liverpool L69 7ZB, UK. [7]Centre for Bioimaging Sciences, National University of Singapore, Singapore 117546, Singapore.
*Corresponding author. Email: b.t.goult@liverpool.ac.uk (B.T.G.); phyyj@nus.edu.sg (J.Y.)
†These authors contributed equally to this work.

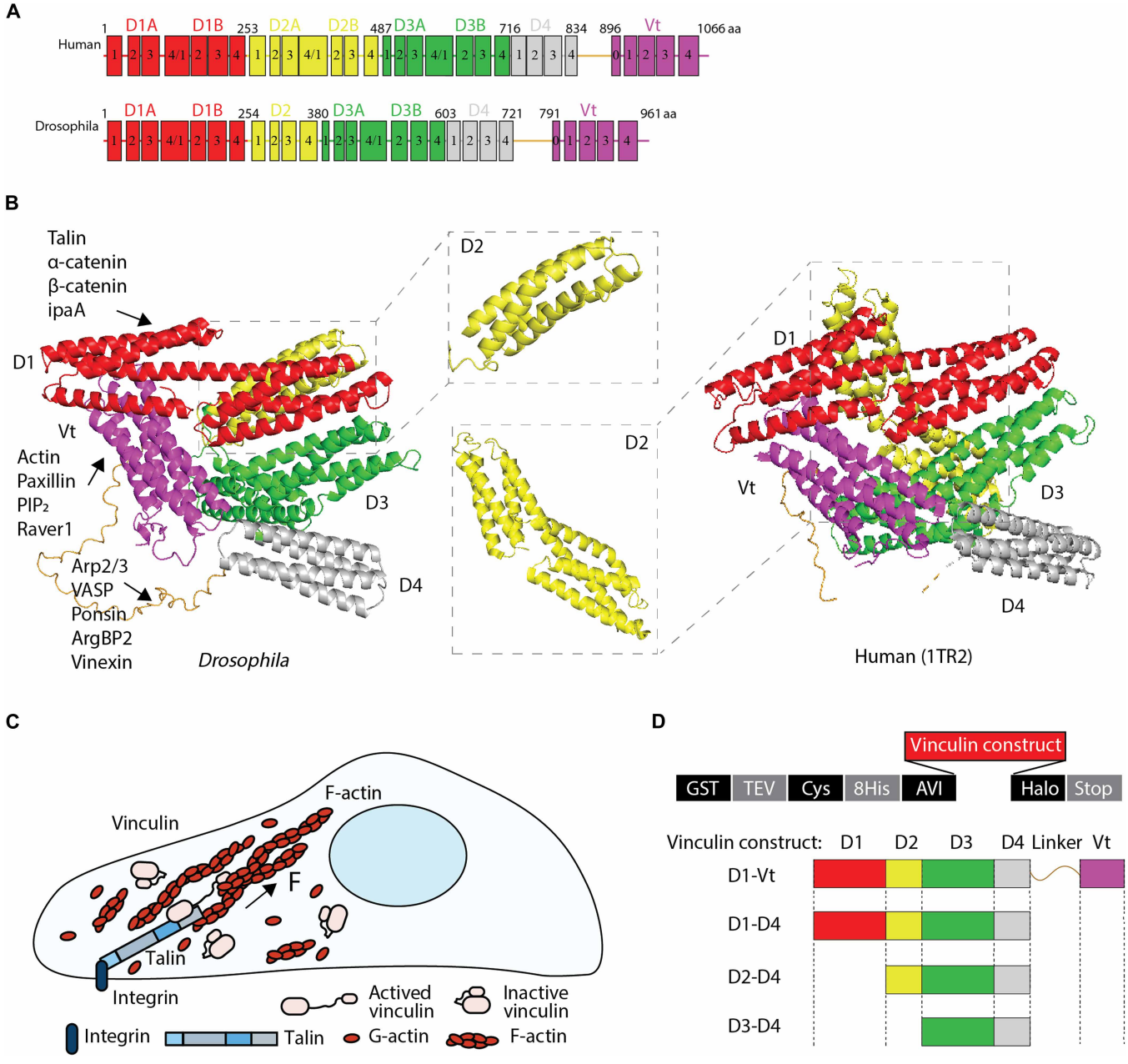

Fig. 1. Stretching vinculin. (**A**) Domain structures of *Drosophila* and human vinculin. The D1 in red, D2 in yellow, D3 in green, D4 in gray, and Vt in purple with linker in gold. (**B**) Structural model of *Drosophila* vinculin predicted by AlphaFold2 in an autoinhibited configuration. Right: The structure of full-length human vinculin (PDB ID 1TR2). Inset: The D2 domains from *Drosophila* vinculin and human vinculin are shown enlarged to highlight the additional domain in human vinculin. *Drosophila* vinculin D2 comprises a single four-helix bundle, whereas D2 from human vinculin is a double four-helix bundle. The known vinculin binding proteins are listed for individual vinculin domains. (**C**) Illustration of the force-transmission supramolecular linkage between integrins engaging the ECM and the actin network mediated by talin (gray/blue) and vinculin (pink). The talin-bound, activated vinculin mediates force transmission from talin to actin. (**D**) The vector design used in these experiments is shown, where a glutathione *S*-transferase (GST) tag is used for purification and, once cleaved using tobacco etch virus (TEV) protease, yields a protein of interest with N-terminal AVI-tag and C-terminal Halo tag for tethering to allow stretching. Four vinculin constructs were designed: D1-Vt (full-length vinculin), D1-D4, D2-D4, and D3-D4. aa, amino acid.

we can predict how tension might influence the binding of factors associated with vinculin.

Our results reveal the complex mechanical response of vinculin and identify that the helical bundles in vinculin exhibit switch-like behavior. We experimentally show that (i) the force-bearing vinculin domains undergo dynamic unfolding and refolding structural transitions over a physiological range of stretching conditions and (ii) the dimensions of the vinculin molecule change dramatically as these domains unfold and refold. Furthermore, results from structural and theoretical modeling suggest that (iii) the vinculin linker is less accessible to binding factors in the autoinhibited conformation and (iv) tensile force of a few piconewtons can extend vinculin

and could notably change the binding affinity between the vinculin linker and its binding factors. Together, this work identifies vinculin as a complex mechanosensor and mechanotransducer.

RESULTS

Mechanical stability of vinculin domains

Our previous work showed that the different domains of the talin rod unfold at different forces and rapidly refold when force is released (*33*). We wished to explore whether vinculin shares these properties and so could also function as a mechanotransducer. Our recent work benefited from the genetic tractability of *Drosophila* for the study of vinculin (*19*), so, for this study, we chose to initiate our single-molecule studies with *Drosophila* vinculin. *Drosophila* vinculin has seven helical bundles (Fig. 1A) and functions at room temperature, as the optimum temperature for *Drosophila* culture is 22° to 25°C. As the structure of *Drosophila* vinculin has not been solved, we predicted it using AlphaFold2 (*34*, *35*), which produced a structure consistent with the structure previously modeled using MODBASE (ref. no. O46037; fig. S1) based on the chicken vinculin crystal structure [Protein Data Bank (PDB) ID 1ST6 (*11*)]. The predicted structure shows high similarity with that of chicken [PDB IDs 1ST6 (*11*) and 6NR7 (*36*)] and human [PDB ID 1TR2 (*10*)] vinculin (Fig. 1, A and B) and also with the vinculin homolog from sponge [PDB ID 6BFI (*37*)]. The main difference between the vinculins from different species is found in the D2 domain (Fig. 1, A and B, insets): The D2 domain in human and chicken vinculin contains two four-helix bundles connected by a long, centrally shared α helix, the D2 domain in *Drosophila* vinculin is a single four-helix bundle, and D2 is absent entirely from sponge vinculin (*37*). The tail domain (Vt) interacts with the head domains, resulting in a compact, lowest-energy autoinhibited, closed conformation (Fig. 1B). When activated, the open form of vinculin links talin to F-actin in the integrin-mediated mechanotransduction pathway, and force is exerted on vinculin (Fig. 1C). Vinculin also interacts with various cellular proteins as indicated (Fig. 1B) (*6*, *22*, *38*–*42*). To understand the mechanical stability of the tension-bearing vinculin domains, we expressed segments of vinculin with suitable tags for stretching (Fig. 1D).

The mechanical response of vinculin

The mechanical stability of *Drosophila* full-length vinculin was investigated at room temperature (24°C) using an in-house constructed magnetic-tweezer setup (Fig. 2A) (*43*, *44*). The height of the end-attached 2.8-μm-diameter superparamagnetic bead (Dynabeads M-270, Invitrogen) was recorded as the force was increased at selected physiologically relevant loading rates in the order of piconewtons per second (*45*–*47*). After each force-loading scan, the force was reduced to 1 pN for 30 s, allowing the unfolded domains to refold, and then, the force-loading scan was repeated. Figure 2B shows representative force-height curves during repeating force loading of a tether containing a full-length vinculin at a loading rate of 2.0 ± 0.2 pN/s. The stepwise bead height increases indicate domain unfolding events. Most of the domains unfold within 7 to 15 pN. The data reveal a complex mechanical response, with six to seven unfolding steps spread over the force range. The number of unfolding steps is consistent with the number of helical bundles (D1A, D1B, D2, D3A, D3B, D4, and Vt). The size of 30 nm of each extension step is also consistent with unfolding of one helical bundle. The data did not reveal a mechanically stable head-tail association, which would have manifested as an additional stepwise bead height increase (see further details in Discussion).

We next examined the mechanical responses of tension-bearing subdomains in *Drosophila* vinculin. In these studies, we reduced the loading rate to 0.40 ± 0.04 pN/s to extend the duration, allowing us to capture more detailed information on the dynamic unfolding and folding fluctuations of these subdomains.

D3-D4 domains

The D4 domain is a single four-helix bundle, and the D3 domain contains two four-helix bundles, D3A and D3B, connected by a shared α helix. Three distinct unfolding steps over a force range of 7 to 15 pN were observed in each scan (Fig. 3A, left) occurring over a range of forces. This indicates that the three α-helix bundles unfold independently. In each cycle, the unfolded D3 and D4 domains refolded with near 100% probability when the force was reduced to 1 pN and held for 30 s, enabling us to perform many mechanical unfolding and refolding cycles of the same domains before breakage.

We next converted the force-dependent step sizes into the contour length of protein peptide released after unfolding (text S1 and fig. S2) to generate a force-contour length scatter plot (Fig. 3A, right). This plot includes more than 700 unfolding events from 13 independent tethers and shows two clear groups (group A and group B) with differential unfolding forces (fig. S3). Group A contains the weakest α-helical bundle, which undergoes rapid reversible

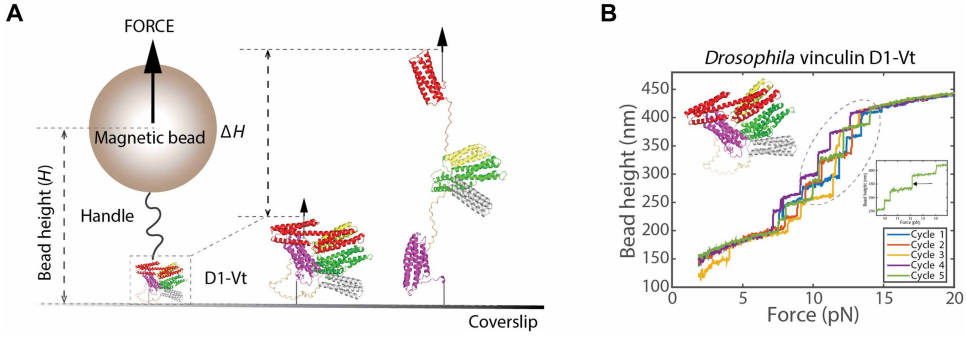

Fig. 2. The mechanical response of full-length vinculin. (**A**) Full-length vinculin (D1-Vt shown in Fig. 1, B and D) is tethered between coverslip and a superparamagnetic bead using a 572–base pair DNA handle. Force is exerted on the bead and onto the protein resulting in a change in bead height (Δ*H*), and domain unfolding events result in stepwise jumps in bead height. (**B**) Five representative consecutive force-height curves obtained from a tether at a loading rate of 2.0 ± 0.2 pN/s. Top left inset: Structural model of full-length *Drosophila* vinculin. Right inset: All of the bundles in vinculin are four-helical except the vinculin tail domain, which is a five-helix bundle making its unfolding event readily identifiable by the larger step that results when it unfolds, indicated by the arrow.

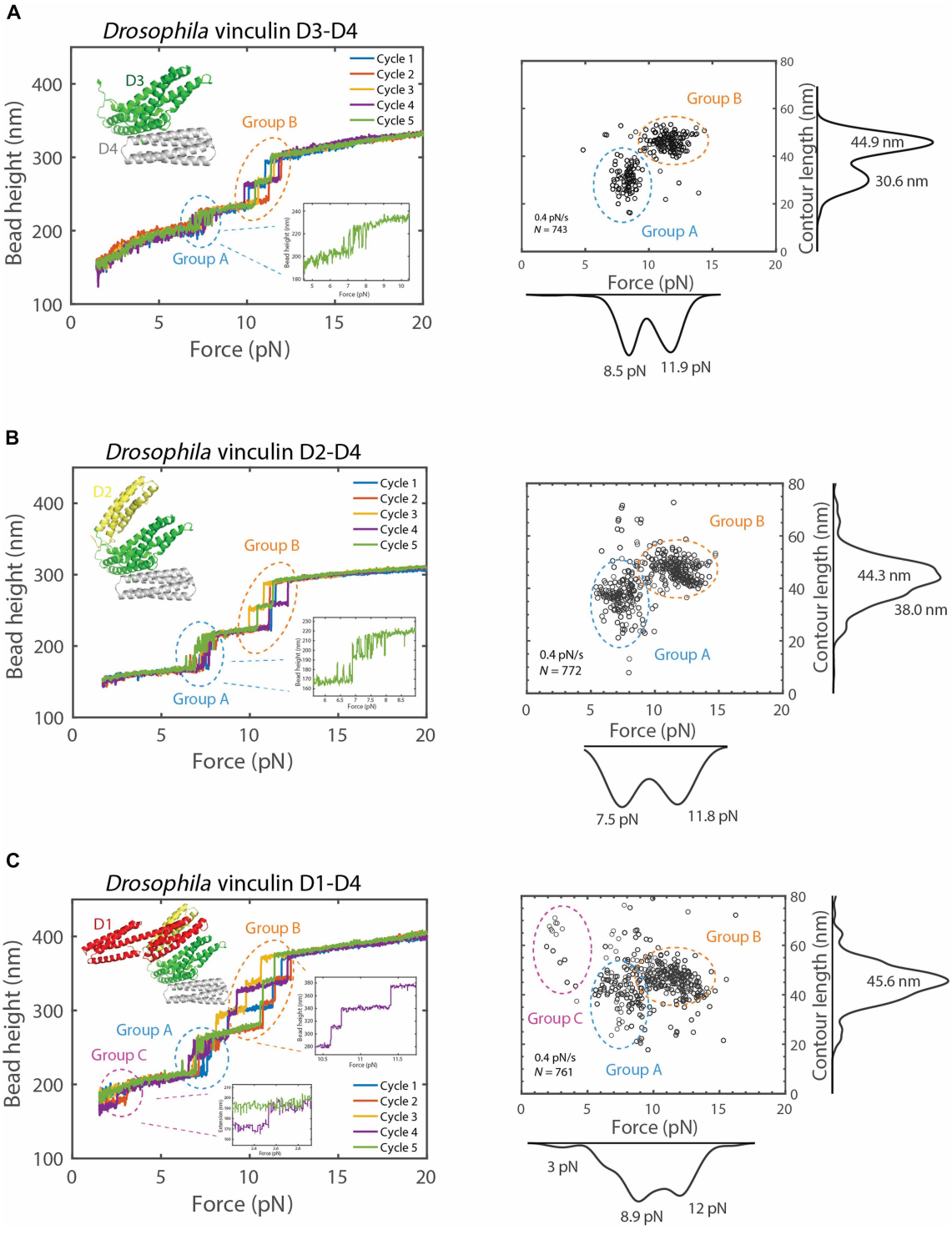

Fig. 3. The mechanical responses of vinculin D3-D4, D2-D4, and D1-D4 subsegments. (**A** to **C**) Five representative, consecutive force-height curves of the unfolding of vinculin D3-D4 (A), D2-D4 (B), and D1-D4 (C) domains at 0.40 ± 0.04 pN/s loading rate are shown. The structural models of each subsegment are shown in the upper left. For each subsegment, the unfolding events are divided into groups based on the contour lengths of released polypeptide polymer and unfolding forces (right). The rapid fluctuations for group A unfolding events are shown enlarged as inset in D3-D4 (A) and D2-D4 domains (B). Two equilibrium unfolding/refolding fluctuations in group A are noted in D2-D4 (B). In the D1-D4 force-extension curves (C), two regions are enlarged corresponding to two unfolding signals from the two four-helix bundles of the D1 domain. For each subsegment, data points are obtained from >700 unfolding events on at least four independent tethers.

unfolding and refolding transitions (Fig. 3A, left) at forces around 8 pN. Similar rapid unfolding/refolding fluctuations were seen previously for the weakest domain in talin, R3 (*16*, *33*), when at 5 pN of force. In contrast, the other two α-helical bundles (group B) unfold at forces of 10 to 15 pN and do not refold at this force, only refolding once force is released at the end of the cycle. This mechanical hysteresis property of the domains was also similar to what was seen in the other talin rod domains (*33*). Assuming independent unfolding of D3 subdomains (D3A and D3B) and D4, as the contour lengths are dependent on the primary sequence of the domain, we could calculate that the group B data in Fig. 3A corresponds to the unfolding of D4 and the larger subdomain from D3, D3B. The group A corresponds to the unfolding of the smaller subdomain in D3, D3A (table S1 and fig. S4).

D2-D4 domains

Having quantified the mechanical response of the D3-D4 domains, we next extended the experiment to include the additional four-helix bundle in the D2 domain. The left panel of Fig. 3B shows the representative force-bead height curves obtained during force-increase scans at the same loading rate of 0.4 pN/s, and the force-contour length scatter plot is shown accordingly (Fig. 3B, right). When compared to the data from D3-D4, the signature of the additional D2 domain is clear. D2 also undergoes rapid reversible unfolding and refolding transitions at forces around 7 to 8 pN. Therefore, the D2 domain is assigned to the mechanical group A.

D1-D4 domains

The results from similar experiments performed for the construct D1-D4 are shown in Fig. 3C. Compared to data obtained from D2-D4, the mechanical signature from D1 is revealed. Two distinct signals from D1 are evident, one contributing to an additional unfolding signal in the mechanical group B; however, D1 domain also contributes to a very mechanically unstable unfolding event, with an unfolding signal at forces around 2 to 3 pN at the loading rate (group C; Fig. 3C). The group C unfolding signal was not observed in every force-increase scan, indicating that the corresponding domain did not always successfully refold when the tether was held at the refolding force (1.0 ± 0.1 pN) over 30 s (fig. S5). The appearance of two distinct unfolding signatures of D1 is consistent with the existence of two α-helical bundles, D1A and D1B, in D1. D1A is responsible for the binding to VBSs, and D1B is a force-bearing α-helical bundle in vinculin-mediated force-transmission pathway. Due to the similar sizes of D1A and D1B, we cannot assign them into the respective group.

Comparing D1 to D4 (Fig. 3C) with full-length vinculin (Fig. 2B), we can identify the additional unfolding step that belongs to the Vt domain, which has a larger force-dependent step size expected from a five-helix bundle. Moreover, the observation that one of the subdomains, either D1A or D1B, did not refold in the majority of the force-loading cycles accounts for the presence of only six unfolding steps in four of the five cycles of stretching full-length vinculin (Fig. 2B).

Overall, the results in this section show that the force-bearing α-helical bundles in the vinculin head domains (D1-D4) show switch-like mechanical properties, unfolding independently over a force range from 2 to 15 pN at the loading rate of 0.4 pN/s. Among the force-bearing domains, we identify two distinct groups of mechanical behaviors, D4, D3B, and a subdomain from D1 are more mechanically stable (group B). Each switch in group B exhibits mechanical hysteresis and does not refold at the same force as it unfolds. The second group (group A) includes the mechanically weaker domains D2 and D3A, which undergo rapid fluctuations in unfolding/refolding around 8 pN of force. At a constant force of approximately 8 pN, D2 and D3A exhibit dynamic structural transitions on a biologically relevant timescale of seconds (fig. S6). While one domain undergoes rapid reversible transitions, which is assigned to D3A because it also appears in Fig. 3A, the other domain (D2) displays one-way unfolding during the constant force application. Together, these results suggest that D2 and D3A can serve as mechanical buffers, extending vinculin's effective force-bearing length by more than 50 nm while maintaining linkage stability over physiologically relevant timescales.

One subdomain in D1 does not fit well into either of these distinct groupings so we included a third group (group C). Notably, the extension of the mechanical linkage mediated by vinculin can change from around 10 nm (low force, relaxed conformation) to more than 150 nm at forces up to 15 pN when all force-bearing domains (D1B, D2, D3, and D4) are unfolded (text S2).

The vinculin linker does not contain force-unfolding steps but is mechanosensitive

Besides the force-bearing vinculin domains, the 59–amino acid linker domain between the vinculin head and tail also bears force. The linker region is not fully visible in the crystal structures solved to date and is predominantly unstructured. As the linker's mechanical response was not visible in our stretching of full-length vinculin (Fig. 2B), we designed an additional construct to allow us to probe how the linker region responds to force. In this construct, the vinculin linker was introduced between two pairs of titin I27 domains, which provide a signature mechanical signal. Single-molecule stretching of the linker region did not show any unfolding steps during force-increase scans, except the signature unfolding steps from the I27 domains (Fig. 4A, inset), which is consistent with the linker being an unstructured polypeptide polymer (Fig. 4A). This is also consistent with the prediction by AlphaFold2 that the vinculin linker is unstructured (Fig. 4B).

Confirming the unstructured nature of the linker, its force-extension curve can be predicted based on the well-known worm-like chain polymer model, with a bending persistence length of 0.8 nm for a proline-rich polypeptide polymer (*48*). The extension of such a flexible polypeptide polymer is sensitive to forces of a few piconewtons, as the linker can be pulled taut at low forces. The linker contains multiple binding sites (Fig. 1B) distributed across its length, and so low forces on vinculin altering the conformation of the binding sites indicate the potential for force sensitivity of the binding of factors to the linker (see Discussion) (*49*).

The conformation of the vinculin linker in the autoinhibited, compact form of *Drosophila* vinculin is likely limited due to the fixed positions of the ends dictated by the folded domains, and the entropic elasticity of an unstructured polypeptide polymer. AlphaFold2 predicts that the linker in the compact conformation of full-length vinculin has a fixed extension of 4.60 ± 0.04 nm (means ± SD) (table S2 and fig. S7). Considering these constraints, the tensile force within the linker can be estimated to be around 3 pN (fig. S8). This tension may pull the linker toward the structural domains (Fig. 4B and movie S1), potentially leading to a less accessible conformation for binding factors, as binding would cause steric clashes with the nearby structured domains. This observation aligns with the full-atom molecular dynamics (MD) simulation of the linker over a 100-ns time frame, beginning with the initial conformation taken from the complete vinculin structure as predicted by AlphaFold2 (movie S1).

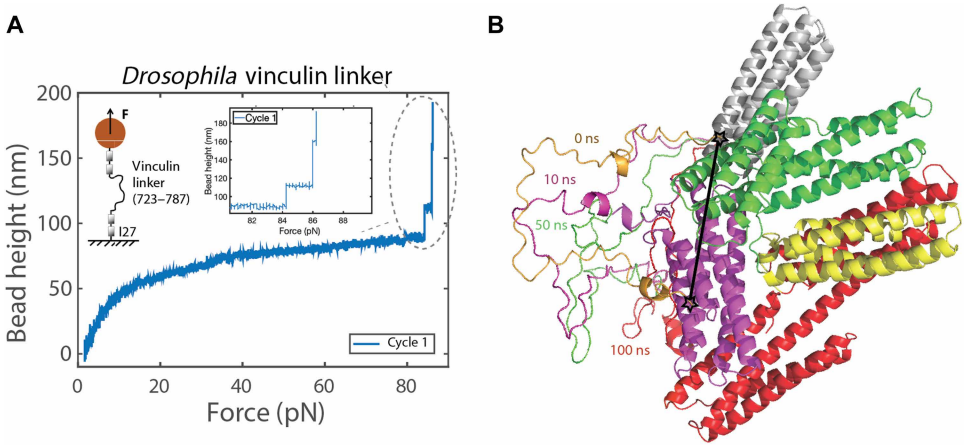

Fig. 4. Vinculin linker is an unstructured polypeptide. (**A**) A representative consecutive force-height curve of a tether containing the vinculin linker is shown. The linker is spanned between two titin I27 domains on each side (inset). The signature unfolding steps of I27 domains serves as a specific control of tether. No unfolding signals were observed from the linker. (**B**) Snapshots of *Drosophila* vinculin linker conformations when relaxed in MD simulation. The initial conformation of the linker (gold) was extracted from the full-length vinculin predicted by AlphaFold2, followed by MD simulation with a fixed end-to-end distance of 4.63 nm for up to 100 ns. The snapshots of the linker conformations extracted at different time points were then added back to the vinculin structure with the same position of the ends (denoted by stars at the ends of the black line) on D4 and Vt.

DISCUSSION

Current models of vinculin show it as a mechanically inert adapter that couples talin/α-catenin to the actin cytoskeleton. In this study, we quantified the mechanical response of vinculin and demonstrated that vinculin is notably more complex mechanically than previously thought. We measured the mechanical stability of the force-bearing domains of vinculin when they are exposed to increasing force at loading rates of 0.4 and 2.0 pN/s. The results indicate that the vinculin helical bundle domains show switch-like behavior and unfold over a range of forces from a few piconewtons to approximately 15 pN at loading rates in the order of piconewtons per second, depending on each domain's mechanical stability. This level of loading rate is physiologically relevant, falling within the range observed for integrins (*45*–*47*). The mechanical stability of the vinculin domains is similar to that of the force-bearing domains in talin or α-catenin at similar loading rates (*16*, *50*).

The vinculin mechanical linkage is mediated via the VD1A domain binding to a VBS in talin or α-catenin, coupled to the actin filaments via the C-terminal Vt domain positioning all the domains from VD1B to VD4 in the force transmission pathway. Each of these domains will be subject to tension. In contrast, the mechanical linkages between VD1 and VBS and Vt and actin do not involve tension on the domain itself but rather on the VD1-VBS and Vt-actin connections themselves, which have been characterized previously (*51*, *52*).

A previous study reported asymmetric vinculin-actin catch-bond kinetics, with lifetimes reaching approximately 10 s at forces of 7 to 10 pN (*52*). Another study showed that, under similar piconewton force ranges, the VD1-VBS complex can remain bound for minutes (*51*). Together, these findings suggest that vinculin-mediated force transmission typically operates on the order of seconds under biologically relevant forces. Our results further demonstrate that, within this force and timescale regime, force-bearing vinculin domains undergo dynamic structural transitions, indicating a potential role for these domains in buffering piconewton forces during dynamic extension changes spanning tens of nanometers.

Our data show that the structural domains of vinculin can withstand tension within a range of a few piconewtons up to 15 pN, at physiological force loading rates. This means that vinculin can buffer tension within this range until all its force-bearing domains are unfolded, corresponding to an extension of up to 150 nm (Fig. 5 and text S2). This buffered tension range aligns with the estimated piconewton tension range measured using Förster resonance energy transfer (FRET) tension sensors in live cells (*30*, *53*). Our previous study also indicated that the tension-dependent structural transitions of talin rod α-helical bundles can buffer the talin tension over a similar range, consistent with the talin tension range reported with FRET tension sensors in live cells (*33*). This suggests that the mechanical unfolding of force-bearing domains can provide an explanation for the physiological tension range for both vinculin and talin in live cells.

In our previous study examining the interactions between full-length vinculin and mechanically exposed VBS, we found that vinculin's autoinhibition is relatively dynamic. This observation is supported by the high binding rate (on the order of 10^6 M^{-1} s^{-1}) and strong binding affinity, as indicated by a dissociation constant (K_d) on the mechanically exposed VBS of approximately 12 nM (*15*). In agreement with these findings, our current study did not reveal a mechanically stable head-tail association, which would have resulted in an additional stepwise extension increase of at least 10 nm at forces of a few piconewtons (text S3 and figs. S9 and S10).

Mechanical regulation of interactions with vinculin

Our findings suggest that the binding of vinculin to its partners is regulated by complex mechanical processes. At the domain level, the switch-like behavior of the vinculin four-helix bundles will displace any proteins that engage the folded conformation and recruit ligands that bind to the open conformation. While the full interactome of vinculin is not known, it is likely that there are ligands for these switch domains in the different states that are recruited as a function of the mechanical signals and the resultant vinculin conformations generated.

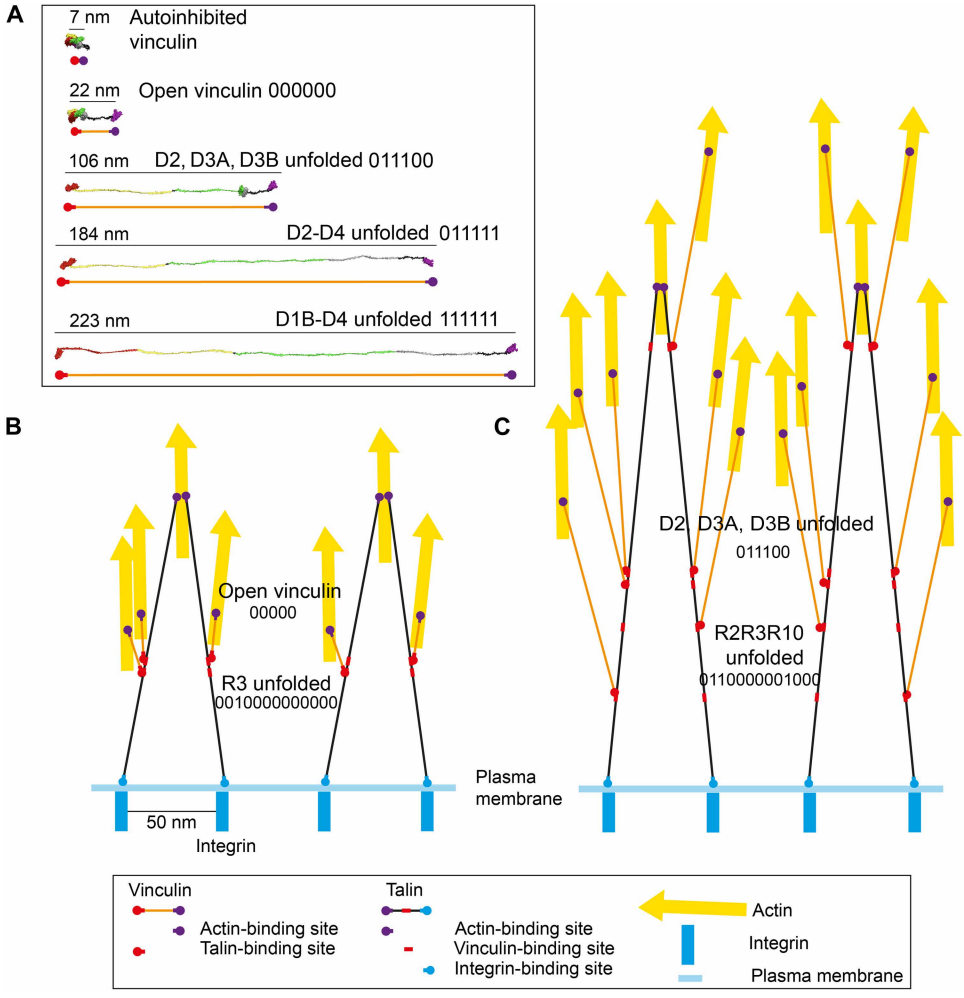

Fig. 5. Vinculin to scale. (**A**) Structural model of vinculin in different states: autoinhibited, open, extended, and fully extended, to show the large differences in dimensions that can occur. The six switch domains: D1B, D2A, D2B, D3A, D3B, and D4, which are in the linkage between the talin-binding site in D1A and the actin-binding site in Vt, are shown in different states. Having two states, folded and unfolded, these domains can be represented as binary switches with states 0 (folded) and 1 (unfolded). The state-dependent contour lengths of vinculin are provided. (**B** and **C**) "To-scale" illustrations of a talin-vinculin-actin linkage in two different mechanical states. (B) With just one talin domain, R3, unfolded and with vinculin open but all domains folded. (C) With three talin domains, R2, R3, and R10, unfolded, and the three weakest domains in vinculin, D2, D3A, and D3B, unfolded. The dimensions of the linkage and the distance between attachment sites can extend to hundreds of nanometers as a function of the switch patterns.

Previous research has shown that the majority of vinculin binding proteins identified so far bind to the unstructured linker region between the head and the tail. Our simulations suggests that in the closed head-tail associated conformation of vinculin, the linker is subjected to a tensile force of around 3 pN pulling it toward the structural domains, which likely reduces the linker's accessibility to its binding factors due to potential steric clashes with the nearby structured domains. The accessibility of binding factors could be further reduced if direct interactions occur between the linker and adjacent domains.

In the open, head-tail dissociated conformation, the linker is positioned farther from the folded structural domains, providing greater accessibility to binding factors. Nonetheless, its binding interactions remain sensitive to force variations within the piconewton range. It is common that binding of a factor to a flexible polymeric binding site, such as DNA or a polypeptide polymer, is associated with distortion conformational changes of the binding site and altered stiffness, resulting in a binding-induced shift in the force-extension curve. Previous theoretical studies have predicted that such binding-induced changes of the force-extension curves can lead to mechanosensitive changes in binding affinity (*48*, *54*, *55*). Theoretically, this leads to these interactions having force-dependent dissociation constants $K_d(F) = K_d^0 e^{-\beta \int_0^F \Delta x(f) df}$, where $\beta = 1/(k_B T)$, F is the applied force, and $\Delta x(f)$ is the change of the force-extension curve upon binding (*49*).

Therefore, forces applied to the flexible vinculin linker could have a substantial impact on the binding of its binding factors in a manner dependent on the specific binding-induced changes of the mechanical properties of the binding sites, which is worthy of future studies. For instance, the embryonic isoform of Drosophila CAP (dCAP-E), a well characterized binder to the vinculin linker, contains two SH3 domains that engage multiple sites on the vinculin

linker (*56*). Here, tension on vinculin will alter both the positioning and flexibility of these sites and would be predicted to modulate the affinity of this interaction.

Overall, these results, in conjunction with previous studies that have shown that vinculin linker binding factors are suppressed from binding to full-length vinculin compared to isolated vinculin linker (*39*, *57*–*59*), suggest that there is a two-layer mechanical regulation of the vinculin linker binding factors: the release of the autoinhibitory conformation of vinculin via binding to mechanically exposed VBS in talin or α-catenin, and the subsequent force-dependent interactions between the vinculin linker and its binding factors.

The changing dimensions of a vinculin linkage

Another observation from this analysis of the switch-like behavior of the vinculin force-bearing domains is that each unfolding event has a large effect on the dimensions of the vinculin molecule. The complete unfolding of the helical bundles in D2-D4 and the linker results in a large extension change (Fig. 2B), and a total of 526 amino acids of peptide polymer will be released under tension. Considering that all the structural domains unfold over tension range from a few piconewtons up to 15 pN under physiologically relevant stretching conditions, the result implies that vinculin tension-bearing domains can buffer tension within this force range during an extension change up to 150 nm (text S2), when it mediates tension transmission from talin or α-catenin to the cytoskeleton network.

Our recent analysis visualizing talin molecules to scale (*60*), changing up to 400 nm at 15 pN, illustrated how these changes in length lead to dramatic reorganization of molecules engaged to these mechanical scaffolds, and here, we show that a similar extension is occurring on the vinculin linkages. The correlation between in vitro extension and in cellulo extensions was shown previously for talin. We previously reported that talin can be extended up to 600 nm when all rod domains are unfolded in single-molecule experiments (*33*), and the Sheetz laboratory showed that talin is extended up to 350 nm in cells (*61*). Future experiments should look at the length of vinculin in cells. Coupling of the large extension changes in talin and the connected vinculin molecules indicates a meshwork of talin and vinculin switches that is incredibly plastic and can adopt numerous different switch patterns and architectures as a result of the mechanical signaling of the cell (Fig. 5, illustration).

In summary, we show that vinculin has a complex mechanical response and has the potential to act as a mechanotransducer as well as a mechanoeffector. As with talin, the vinculin domains unfold at physiological forces, and the changes in dimensions of the linkages between talin and actin mediated by vinculin as well as the proteins recruited to that site will be dependent on the mechanically induced conformations of each vinculin molecule.

MATERIALS AND METHODS

Materials and magnetic tweezers

The Halo-tagged *Drosophila* vinculin constructs (D3-D4, D2-D4, D1-D4, and D1-Vt) were made as described previously (*33*) using a custom vector comprising an N-terminal glutathione *S*-transferase (GST) tag for protein purification, which was cleaved using tobacco etch virus (TEV) protease, to yield vinculin proteins with N-terminal AVI-tag and C-terminal Halo tags. An in-house–made magnetic tweezer apparatus was used in this study with the paramagnetic beads (catalog no. AP-25-10, Spherotech) attached with short dsDNA handles (*33*). In the force scanning process, forces were incrementally increased with different scan rates.

AlphaFold2 protein structure prediction

The amino acid sequences of the full-length *Drosophila* vinculin (UniProt O46037 VINC _DROME) and its linker (amino acids 728 to 786) were used for AlphaFold2 protein structure prediction using ColabFold (*34*, *35*), and the structural models were analyzed using PyMOL software (PyMOL Molecular Graphics System, Version 2.0, Schrödinger, LLC). The structural models were validated by comparison with the crystal structure of human full-length vinculin (PDB ID 1TR2) (*11*).

MD simulations

Drosophila vinculin linker conformations were generated using MD simulations. GROMACS 2019.6 (*62*, *63*) was used with an initial protein complex predicted by AlphaFold2 (*34*, *35*). These simulations were performed under the AMBER99SB-ILDN force field (*64*) with the extended simple point charge (SPC/E) water model (*65*). The initial complex was immersed in a periodic cubic box filled with 0.15 M NaCl solution. The steepest descent minimization of 50,000 steps was followed by a 100-ps NPT (isothermal-isobaric ensemble) and a 100-ps NVT (canonical ensemble; 300 K) equilibration. Subsequently, a 100-ns MD simulation was performed with the system coordinates saved every 10 ps for further analysis.

Supplementary Materials

The PDF file includes:

Text S1 to S3
Figs. S1 to S10
Tables S1 and S2
Legend for movie S1
References

Other Supplementary Material for this manuscript includes the following:

Movie S1

REFERENCES AND NOTES

1. M. Michael, M. Parsons, New perspectives on integrin-dependent adhesions. *Curr. Opin. Cell Biol.* **63**, 31–37 (2020).
2. A. Angulo-Urarte, T. van der Wal, S. Huveneers, Cell-cell junctions as sensors and transducers of mechanical forces. *Biochim. Biophys. Acta Biomembr.* **1862**, 183316 (2020).
3. B. T. Goult, N. H. Brown, M. A. Schwartz, Talin in mechanotransduction and mechanomemory at a glance. *J. Cell Sci.* **134**, jcs258749 (2021).
4. W. H. Goldmann, Role of vinculin in cellular mechanotransduction. *Cell Biol. Int.* **40**, 241–256 (2016).
5. B. Klapholz, N. H. Brown, Talin–The master of integrin adhesions. *J. Cell Sci.* **130**, 2435–2446 (2017).
6. J. L. Bays, K. A. DeMali, Vinculin in cell–cell and cell–matrix adhesions. *Cell. Mol. Life Sci.* **74**, 2999–3009 (2017).
7. P. Atherton, B. Stutchbury, D. Jethwa, C. Ballestrem, Mechanosensitive components of integrin adhesions: Role of vinculin. *Exp. Cell Res.* **343**, 21–27 (2016).
8. Y. Guo, J. Yan, B. T. Goult, Mechanotransduction through protein stretching. *Curr. Opin. Cell Biol.* **87**, 102327 (2024).
9. R. Janoštiak, J. Brábek, V. Auernheimer, Z. Tatárová, L. A. Lautscham, T. Dey, J. Gemperle, R. Merkel, W. H. Goldmann, B. Fabry, D. Rösel, CAS directly interacts with vinculin to control mechanosensing and focal adhesion dynamics. *Cell. Mol. Life Sci.* **71**, 727–744 (2014).
10. B. T. Goult, T. Zacharchenko, N. Bate, R. Tsang, F. Hey, A. R. Gingras, P. R. Elliott, G. C. K. Roberts, C. Ballestrem, D. R. Critchley, I. L. Barsukov, RIAM and vinculin binding to talin are mutually exclusive and regulate adhesion assembly and turnover. *J. Biol. Chem.* **288**, 8238–8249 (2013).
11. R. A. Borgon, C. Vonrhein, G. Bricogne, P. R. Bois, T. Izard, Crystal structure of human vinculin. *Structure* **12**, 1189–1197 (2004).

12. C. Bakolitsa, D. M. Cohen, L. A. Bankston, A. A. Bobkov, G. W. Cadwell, L. Jennings, D. R. Critchley, S. W. Craig, R. C. Liddington, Structural basis for vinculin activation at sites of cell adhesion. *Nature* **430**, 583–586 (2004).
13. R. P. Johnson, S. W. Craig, F-actin binding site masked by the intramolecular association of vinculin head and tail domains. *Nature* **373**, 261–264 (1995).
14. D. S. Chorev, T. Volberg, A. Livne, M. Eisenstein, B. Martins, Z. Kam, B. M. Jockusch, O. Medalia, M. Sharon, B. Geiger, Conformational states during vinculin unlocking differentially regulate focal adhesion properties. *Sci. Rep.* **8**, 2693 (2018).
15. Y. Wang, M. Yao, K. B. Baker, R. E. Gough, S. Ie, B. T. Goult, J. Yan, Force-dependent interactions between talin and full-length vinculin. *J. Am. Chem. Soc.* **143**, 14726–14737 (2021).
16. M. Yao, B. T. Goult, H. Chen, P. Cong, M. P. Sheetz, J. Yan, Mechanical activation of vinculin binding to talin locks talin in an unfolded conformation. *Sci. Rep.* **4**, 4610 (2014).
17. S. M. Pang, S. Le, A. V. Kwiatkowski, J. Yan, Mechanical stability of αT-catenin and its activation by force for vinculin binding. *Mol. Biol. Cell* **30**, 1930–1937 (2019).
18. D. W. Dumbauld, T. T. Lee, A. Singh, J. Scrimgeour, C. A. Gersbach, E. A. Zamir, J. Fu, C. S. Chen, J. E. Curtis, S. W. Craig, A. J. García, How vinculin regulates force transmission. *Proc. Natl. Acad. Sci. U.S.A.* **110**, 9788–9793 (2013).
19. A. P. Maartens, J. Wellmann, E. Wictome, B. Klapholz, H. Green, N. H. Brown, *Drosophila* vinculin is more harmful when hyperactive than absent, and can circumvent integrin to form adhesion complexes. *J. Cell Sci.* **129**, 4354–4365 (2016).
20. R. M. Ezzell, W. H. Goldmann, N. Wang, N. Parasharama, D. E. Ingber, Vinculin promotes cell spreading by mechanically coupling integrins to the cytoskeleton. *Exp. Cell Res.* **231**, 14–26 (1997).
21. F. J. Alenghat, B. Fabry, K. Y. Tsai, W. H. Goldmann, D. E. Ingber, Analysis of cell mechanics in single vinculin-deficient cells using a magnetic tweezer. *Biochem. Biophys. Res. Commun.* **277**, 93–99 (2000).
22. J. D. Humphries, P. Wang, C. Streuli, B. Geiger, M. J. Humphries, C. Ballestrem, Vinculin controls focal adhesion formation by direct interactions with talin and actin. *J. Cell Biol.* **179**, 1043–1057 (2007).
23. C. Le Clainche, S. P. Dwivedi, D. Didry, M.-F. Carlier, Vinculin is a dually regulated actin filament barbed end-capping and side-binding protein. *J. Biol. Chem.* **285**, 23420–23432 (2010).
24. I. Thievessen, P. M. Thompson, S. Berlemont, K. M. Plevock, S. V. Plotnikov, A. Zemljic-Harpf, R. S. Ross, M. W. Davidson, G. Danuser, S. L. Campbell, C. M. Waterman, Vinculin–actin interaction couples actin retrograde flow to focal adhesions, but is dispensable for focal adhesion growth. *J. Cell Biol.* **202**, 163–177 (2013).
25. L. B. Case, M. A. Baird, G. Shtengel, S. L. Campbell, H. F. Hess, M. W. Davidson, C. M. Waterman, Molecular mechanism of vinculin activation and nanoscale spatial organization in focal adhesions. *Nat. Cell Biol.* **17**, 880–892 (2015).
26. R. B. Hazan, L. Kang, S. Roe, P. I. Borgen, D. L. Rimm, Vinculin is associated with the E-cadherin adhesion complex. *J. Biol. Chem.* **272**, 32448–32453 (1997).
27. E. E. Weiss, M. Kroemker, A.-H. Rüdiger, B. M. Jockusch, M. Rüdiger, Vinculin is part of the cadherin–catenin junctional complex: Complex formation between α-catenin and vinculin. *J. Cell Biol.* **141**, 755–764 (1998).
28. W. H. Goldmann, V. Auernheimer, I. Thievessen, B. Fabry, Vinculin, cell mechanics and tumour cell invasion. *Cell Biol. Int.* **37**, 397–405 (2013).
29. R. Biswas, A. Banerjee, S. Lembo, Z. Zhao, V. Lakshmanan, R. Lim, S. Ie, M. Nakasaki, V. Kutyavin, G. Wright, D. Palakodeti, R. S. Ross, C. Jamora, V. Vasioukhin, Y. Jie, S. Raghavan, Mechanical instability of adherens junctions overrides intrinsic quiescence of hair follicle stem cells. *Dev. Cell* **56**, 761–780.e7 (2021).
30. V. Kanoldt, C. Kluger, C. Barz, A. L. Schweizer, D. Ramanujam, L. Windgasse, S. Engelhardt, A. Chrostek-Grashoff, C. Grashoff, Metavinculin modulates force transduction in cell adhesion sites. *Nat. Commun.* **11**, 6403 (2020).
31. V. C. Vasile, M. L. Will, S. R. Ommen, W. D. Edwards, T. M. Olson, M. J. Ackerman, Identification of a metavinculin missense mutation, R975W, associated with both hypertrophic and dilated cardiomyopathy. *Mol. Genet. Metab.* **87**, 169–174 (2006).
32. M. Maeda, E. Holder, B. Lowes, S. Valent, R. D. Bies, Dilated cardiomyopathy associated with deficiency of the cytoskeletal protein metavinculin. *Circulation* **95**, 17–20 (1997).
33. M. Yao, B. T. Goult, B. Klapholz, X. Hu, C. P. Toseland, Y. Guo, P. Cong, M. P. Sheetz, J. Yan, The mechanical response of talin. *Nat. Commun.* **7**, 11966 (2016).
34. A. W. Senior, R. Evans, J. Jumper, J. Kirkpatrick, L. Sifre, T. Green, C. Qin, A. Žídek, A. W. R. Nelson, A. Bridgland, H. Penedones, S. Petersen, K. Simonyan, S. Crossan, P. Kohli, D. T. Jones, D. Silver, K. Kavukcuoglu, D. Hassabis, Improved protein structure prediction using potentials from deep learning. *Nature* **577**, 706–710 (2020).
35. J. Jumper, R. Evans, A. Pritzel, T. Green, M. Figurnov, O. Ronneberger, K. Tunyasuvunakool, R. Bates, A. Žídek, A. Potapenko, A. Bridgland, C. Meyer, S. A. A. Kohl, A. J. Ballard, A. Cowie, B. Romera-Paredes, S. Nikolov, R. Jain, J. Adler, T. Back, S. Petersen, D. Reiman, E. Clancy, M. Zielinski, M. Steinegger, M. Pacholska, T. Berghammer, S. Bodenstein, D. Silver, O. Vinyals, A. W. Senior, K. Kavukcuoglu, P. Kohli, D. Hassabis, Highly accurate protein structure prediction with AlphaFold. *Nature* **596**, 583–589 (2021).
36. D. L. Stec, B. Stec, Complete model of vinculin suggests the mechanism of activation by helical super-bundle unfurling. *Protein J.* **41**, 55–70 (2022).
37. P. W. Miller, S. Pokutta, J. M. Mitchell, J. V. Chodaparambil, D. N. Clarke, W. J. Nelson, W. I. Weis, S. A. Nichols, Analysis of a vinculin homolog in a sponge (phylum Porifera) reveals that vertebrate-like cell adhesions emerged early in animal evolution. *J. Biol. Chem.* **293**, 11674–11686 (2018).
38. W. H. Ziegler, R. C. Liddington, D. R. Critchley, The structure and regulation of vinculin. *Trends Cell Biol.* **16**, 453–460 (2006).
39. K. A. DeMali, C. A. Barlow, K. Burridge, Recruitment of the Arp2/3 complex to vinculin: Coupling membrane protrusion to matrix adhesion. *J. Cell Biol.* **159**, 881–891 (2002).
40. N. Kioka, S. Sakata, T. Kawauchi, T. Amachi, S. K. Akiyama, K. Okazaki, C. Yaen, K. M. Yamada, S. I. Aota, Vinexin: A novel vinculin-binding protein with multiple SH3 domains enhances actin cytoskeletal organization. *J. Cell Biol.* **144**, 59–69 (1999).
41. N. P. Brindle, M. R. Holt, J. E. Davies, C. J. Price, D. R. Critchley, The focal-adhesion vasodilator-stimulated phosphoprotein (VASP) binds to the proline-rich domain in vinculin. *Biochem. J.* **318**, 753–757 (1996).
42. H.-J. Choi, S. Pokutta, G. W. Cadwell, A. A. Bobkov, L. A. Bankston, R. C. Liddington, W. I. Weis, αE-catenin is an autoinhibited molecule that coactivates vinculin. *Proc. Natl. Acad. Sci.* **109**, 8576–8581 (2012).
43. H. Chen, H. Fu, X. Zhu, P. Cong, F. Nakamura, J. Yan, Improved high-force magnetic tweezers for stretching and refolding of proteins and short DNA. *Biophys. J.* **100**, 517–523 (2011).
44. X. Zhao, X. Zeng, C. Lu, J. Yan, Studying the mechanical responses of proteins using magnetic tweezers. *Nanotechnology* **28**, 414002 (2017).
45. J. D. Combs, A. K. Foote, H. Ogasawara, A. Velusamy, S. A. Rashid, J. N. Mancuso, K. Salaita, Measuring integrin force loading rates using a two-step DNA tension sensor. *J. Am. Chem. Soc.* **146**, 23034–23043 (2024).
46. Y. Hu, H. Li, C. Zhang, J. Feng, W. Wang, W. Chen, M. Yu, X. Liu, X. Zhang, Z. Liu, DNA-based ForceChrono probes for deciphering single-molecule force dynamics in living cells. *Cell* **187**, 3445–3459.e15 (2024).
47. M. H. Jo, P. Meneses, O. Yang, C. C. Carcamo, S. Pangeni, T. Ha, Determination of single-molecule loading rate during mechanotransduction in cell adhesion. *Science* **383**, 1374–1379 (2024).
48. M. Yu, S. Ie, A. K. Efremov, X. Zeng, A. Bershadsky, J. Yan, Effects of mechanical stimuli on profilin-and formin-mediated actin polymerization. *Nano Lett.* **18**, 5239–5247 (2018).
49. Y. Wang, J. Yan, B. T. Goult, Force-dependent binding constants. *Biochemistry* **58**, 4696–4709 (2019).
50. M. Yao, W. Qiu, R. Liu, A. K. Efremov, P. Cong, R. Seddiki, M. Payre, C. T. Lim, B. Ladoux, R. M. Mège, J. Yan, Force-dependent conformational switch of α-catenin controls vinculin binding. *Nat. Commun.* **5**, 4525 (2014).
51. S. Le, M. Yu, J. Yan, Direct single-molecule quantification reveals unexpectedly high mechanical stability of vinculin-talin/ α-catenin linkages. *Sci. Adv.* **5**, eaav2720 (2019).
52. D. L. Huang, N. A. Bax, C. D. Buckley, W. I. Weis, A. R. Dunn, Vinculin forms a directionally asymmetric catch bond with F-actin. *Science* **357**, 703–706 (2017).
53. C. Grashoff, B. D. Hoffman, M. D. Brenner, R. Zhou, M. Parsons, M. T. Yang, M. A. McLean, S. G. Sligar, C. S. Chen, T. Ha, M. A. Schwartz, Measuring mechanical tension across vinculin reveals regulation of focal adhesion dynamics. *Nature* **466**, 263–266 (2010).
54. A. Y. Alexandrova, K. Arnold, S. Schaub, J. M. Vasiliev, J. J. Meister, A. D. Bershadsky, A. B. Verkhovsky, Comparative dynamics of retrograde actin flow and focal adhesions: Formation of nascent adhesions triggers transition from fast to slow flow. *PLOS ONE* **3**, e3234 (2008).
55. V. Swaminathan, J. M. Kalappurakkal, S. B. Mehta, P. Nordenfelt, T. I. Moore, N. Koga, D. A. Baker, R. Oldenbourg, T. Tani, S. Mayor, T. A. Springer, C. M. Waterman, Actin retrograde flow actively aligns and orients ligand-engaged integrins in focal adhesions. *Proc. Natl. Acad. Sci. U.S.A.* **114**, 10648–10653 (2017).
56. R. Bharadwaj, M. Roy, T. Ohyama, E. Sivan-Loukianova, M. Delannoy, T. E. Lloyd, M. Zlatic, D. F. Eberl, A. L. Kolodkin, Cbl-associated protein regulates assembly and function of two tension-sensing structures in *Drosophila*. *Development* **140**, 627–638 (2013).
57. H. Chen, D. M. Cohen, D. M. Choudhury, N. Kioka, S. W. Craig, Spatial distribution and functional significance of activated vinculin in living cells. *J. Cell Biol.* **169**, 459–470 (2005).
58. S. Hüttelmaier, O. Mayboroda, B. Harbeck, T. Jarchau, B. M. Jockusch, M. Rüdiger, The interaction of the cell-contact proteins VASP and vinculin is regulated by phosphatidylinositol-4, 5-bisphosphate. *Curr. Biol.* **8**, 479–488 (1998).
59. L. Sun, J. K. Noel, H. Levine, J. N. Onuchic, Molecular simulations suggest a force-dependent mechanism of vinculin activation. *Biophys. J.* **113**, 1697–1710 (2017).
60. S. F. Barnett, B. T. Goult, The MeshCODE to scale—Visualising synaptic binary information. *Front. Cell. Neurosci.* **16**, 1014629 (2022).
61. F. Margadant, L. L. Chew, X. Hu, H. Yu, N. Bate, X. Zhang, M. Sheetz, Mechanotransduction in vivo by repeated talin stretch-relaxation events depends upon vinculin. *PLoS Biol.* **9**, e1001223 (2011).
62. M. J. Abraham, T. Murtola, R. Schulz, S. Páll, J. C. Smith, B. Hess, E. Lindahl, GROMACS: High performance molecular simulations through multi-level parallelism from laptops to supercomputers. *SoftwareX* **1**, 19–25 (2015).

63. C. Tan, J. Jung, C. Kobayashi, D. U. L. Torre, S. Takada, Y. Sugita, Implementation of residue-level coarse-grained models in GENESIS for large-scale molecular dynamics simulations. *PLoS Comput. Biol.* **18**, e1009578 (2022).
64. K. Lindorff-Larsen, S. Piana, K. Palmo, P. Maragakis, J. L. Klepeis, R. O. Dror, D. E. Shaw, Improved side-chain torsion potentials for the Amber ff99SB protein force field. *Proteins* **78**, 1950–1958 (2010).
65. H. J. Berendsen, J.-R. Grigera, T. P. Straatsma, The missing term in effective pair potentials. *J. Phys. Chem.* **91**, 6269–6271 (1987).
66. H. Chen, G. Yuan, R. S. Winardhi, M. Yao, I. Popa, J. M. Fernandez, J. Yan, Dynamics of equilibrium folding and unfolding transitions of titin immunoglobulin domain under constant forces. *J. Am. Chem. Soc.* **137**, 3540–3546 (2015).
67. R. S. Winardhi, Q. Tang, J. Chen, M. Yao, J. Yan, Probing small molecule binding to unfolded polyprotein based on its elasticity and refolding. *Biophys. J.* **111**, 2349–2357 (2016).
68. J. F. Marko, E. D. Siggia, Stretching DNA. *Macromolecules* **28**, 8759–8770 (1995).

Acknowledgments
Funding: This research is supported by the Singapore Ministry of Education Academic Research Funds Tier 1 (24-1547-A0001 to J.Y.), Singapore Ministry of Education Academic Research Funds Tier 2 (MOE-T2EP50123-0008 to J.Y.), Singapore Ministry of Education Academic Research Funds Tier 3 (MOE-MOET32021-0003 to J.Y.), National Research Foundation (NRF) Singapore, Mechanobiology Institute under its Mid-Sized Grant (MSG) (NRF-MSG-2023-0001 to J.Y.), National University of Singapore through the Mechanobiology Institute (A-0003467-00-00 to J.Y.), BBSRC (BB/S007245/1 to B.T.G. and N.H.B. and BB/S007318/1 to N.H.B.), and Cancer Research UK (CRUK-A21671 to B.T.G.). **Author contributions:** J.Y., Y.W., M.Y., B.T.G., and N.H.B. conceived the research. X.L., J.L., and Y.W. performed the experiments and analyzed the data. B.K. generated reagents and stretchable protein fragments. K.B.B. contributed to investigation and data curation. X.L., J.L., Y.W., B.T.G., and J.Y. wrote the manuscript with help from all authors. J.Y., B.T.G., and N.H.B. supervised the research. **Competing interests:** The authors declare that they have no competing interests. **Data and materials availability:** All data needed to evaluate the conclusions in the paper are present in the paper and/or the Supplementary Materials.

Submitted 29 May 2025
Accepted 29 September 2025
Published 31 October 2025
10.1126/sciadv.ady6949